ISPRS Journal of Photogrammetry and Remote Sensing 130 (2017) 246–255

Contents lists available at ScienceDirect

ISPRS Journal of Photogrammetry and Remote Sensing

journal homepage: www.elsevier.com/locate/isprsjprs

Predicting grain yield in rice using multi-temporal vegetation indices from UAV-based multispectral and digital imagery

X. Zhou, H.B. Zheng, X.Q. Xu, J.Y. He, X.K. Ge, X. Yao, T. Cheng, Y. Zhu, W.X. Cao, Y.C. Tian *

National Engineering and Technology Center for Information Agriculture, Jiangsu Key Laboratory for Information Agriculture, Nanjing Agricultural University, 1 Weigang Road, Nanjing, Jiangsu 210095, PR China

ARTICLE INFO

Article history:
Received 13 August 2016
Received in revised form 13 December 2016
Accepted 3 May 2017

Keywords:
UAVs
Multispectral image
Digital image
Grain yield prediction
Rice

ABSTRACT

Timely and non-destructive assessment of crop yield is an essential part of agricultural remote sensing (RS). The development of unmanned aerial vehicles (UAVs) has provided a novel approach for RS, and makes it possible to acquire high spatio-temporal resolution imagery on a regional scale. In this study, the rice grain yield was predicted with single stage vegetation indices (VIs) and multi-temporal VIs derived from the multispectral (MS) and digital images. The results showed that the booting stage was identified as the optimal stage for grain yield prediction with VIs at a single stage for both digital image and MS image. And corresponding optimal color index was VARI with R^2 value of 0.71 (Log relationship). While the optimal vegetation index $NDVI_{[800,720]}$ based on MS images showed a linear relationship with the grain yield and gained a higher R^2 value (0.75) than color index did. The multi-temporal VIs showed a higher correlation with grain yield than the single stage VIs did. And the VIs at two random growth stage with the multiple linear regression function [MLR(VI)] performed best. The highest correlation coefficient were 0.76 with $MLR(NDVI_{[800,720]})$ at the booting and heading stages (for the MS image) and 0.73 with MLR(VARI) at the jointing and booting stages (for the digital image). In addition, the VIs that showed a high correlation with LAI performed well for yield prediction, and the VIs composed of red edge band (720 nm) and near infrared band (800 nm) were found to be more effective in predicting yield and LAI at high level. In conclusion, this study has demonstrated that both MS and digital sensors mounted on the UAV are reliable platforms for rice growth and grain yield estimation, and determined the best period and optimal VIs for rice grain yield prediction.

1. Introduction

Yield in grain crops is one of the most important issues related to national food security and personal living standards (Wang et al., 2014). Timely and accurate crop yield forecasts prior to harvest enable planners to make national food policy more reasonable (Noureldin et al., 2013). Traditionally, crop yield prediction has relied on ground-based field surveys, which are costly and prone to poor crop assessment (Reynolds et al., 2000). Therefore, developing a low-cost, rapid, and accurate method for grain yield prediction at a regional scale is a vital goal for crop production (Panda et al., 2010).

Remote sensing (RS) technology is an effective means to monitor crop growth parameters such as biomass (Fu et al., 2014), leaf area index (LAI) (Haboudane et al., 2004; Verger et al., 2014; Liang et al., 2015), and chlorophyll content (Haboudane et al., 2002), which can be estimated accurately with the vegetation indices (VIs). A series of studies have addressed crop yield prediction (Moran et al., 1997). Tucker et al. (1980) showed that there is a linear relationship between the normalized difference vegetation index (NDVI) and grain yield in wheat. Wang et al. (2010) derived yield prediction models with canopy reflectance band ratios (NIR/RED, NIR/GRN) at booting stage from field measurements, and these models have successfully forecasted the large-area rice yield with the satellite images. The Becker-Reshef et al. (2010) forecasted the wheat yield in Kansas and Ukraine with time series NDVI data from the moderate resolution imaging spectroradiometer (MODIS). And multi-temple VIs were proposed to improve the yield prediction accuracy (Xue et al., 2007). Wang et al. (2014) predicted wheat yield with the accumulated VIs such as ∑NDVI(Nir,

* Corresponding author.
E-mail addresses: x_zhou1989@163.com (X. Zhou), 2015201019@njau.edu.cn (H.B. Zheng), 2015101043@njau.edu.cn (X.Q. Xu), 2015201015@njau.edu.cn (J.Y. He), 2015101041@njau.edu.cn (X.K. Ge), yaoxia@njau.edu.cn (X. Yao), yanzhu@njau.edu.cn (T. Cheng), caow@njau.edu.cn (Y. Zhu), tcheng@njau.edu.cn (W.X. Cao), yctian@njau.edu.cn (Y.C. Tian).

http://dx.doi.org/10.1016/j.isprsjprs.2017.05.003
0924-2716/

Green) and ∑RVI(Nir, Red) from jointing to the initial filling stage, and achieved a higher prediction accuracy than with VI at a single stage. While it is hard to acquire adequate data from the satellite, the accumulated VIs were the only form used. Another method for forecasting yield uses yield-related agronomic parameters that can be estimated from RS data. Researchers have estimated the absorbed photosynthetically active radiation (PAR) and LAI from RS data and used it to predict yield (Pradhan et al., 2014; Sibley et al., 2014).

Satellite images from Landsat, SPOT5, and Quickbird with high spatial resolution of 30 m, 10 m, and 3 m overcame the disadvantage of small survey regions and showed a high level of accuracy for crop yield prediction (Hamar et al., 1996; Yang et al., 2006, 2009). However, in the south China, the small plots, complex terrain, and cloudy cover during the rice growth stages and high cost are greatly limit the application of satellite imagery. The recent technological advancements in unmanned aerial vehicles (UAV), and the miniaturization of sensors has field the current explosion of their application to precision agriculture. Based on UAV system, high spatio-temporal resolution remotely sensed data can be acquired for crop monitoring in a low-cost and more practical way (Zhang and Kovacs, 2012; Verger et al., 2014).

Several sensors have been installed on UAVs for crop growth monitoring and plant cover, disease detection (Córcoles et al., 2013; Garcia-Ruiz et al., 2013; Hunt et al., 2005). Multispectral (MS) and hyperspectral (HS) cameras have been widely used to monitor plant growth and biochemical indicators for many options of vegetation indices (Li et al., 2012; Zarco-Tejada et al., 2012; Verger et al., 2014). Zarco-Tejada et al. (2013) combined R_{515}/R_{570} and TCARI/OSAVI narrow-band indices for the leaf carotenoid estimation with a hyperspectral camera onboard UAV. And Stagakis et al. (2012) have successfully estimated the water stress for citrus orchard with PRI_{515} and PRI_{570} from MS image. The digital camera has also been widely used for its high spatial resolution and low price (Córcoles et al., 2013). Classification of the RGB image acquired from digital camera have been a powerful tool for plant cover detection (Córcoles et al., 2013). In addition, A large number of studies have derived the color index from digital images for crop growth monitoring (Hunt et al., 2005). Torres-Sánchez et al. (2014) used the color index such as Excess green (ExG), Vegetative (VEG) calculated from the RGB images for vegetation fraction mapping, and achieved good accuracy with the value ranging from 89.33% to 91.99%. Jannoura et al. (2015) reported that normalized Green-Red difference index (NGRDI) derived from the RGB image was positively and significantly correlated with the aboveground biomass of peas and oats with R^2 ranging from 0.58 to 0.78.

UAV platform can provide high spatio-temporal resolution images for agricultural RS, and some of exploratory researches have conducted for yield prediction. Swain et al. (2010) proved that NDVI at panicle initiation stage calculated from the UAVs was highly correlated with rice yield and Teoh et al. (2016) also successfully estimated the yield with the NDVI and band R, G. But in these studies, the limited datasets were acquired at one single stage, and the model was developed based on NDVI which easily saturated when the canopy is dense (Liang, 2004). Some studies also tried to predict crop yield with the plant height. Crop surface models (CSMs) have been developed for crop height determination based on the digital images (Bendig et al., 2014, 2015; Geipel et al., 2014). However, the crop yield–height relationship usually varies with rice cultivars under different crop growth status. In addition, fewer studies focused on estimating crop yield with the color index derived from the UAVs. VIs derived from multispectral images and digital images showed sensitivities to crop growth status and canopy structure. The performance and potential of these VIs for crop yield prediction should be further tested. LAI is an important parameter that indicates crop photosynthesis and growth status and is of significance for crop yield prediction (Noureldin et al., 2013; Verger et al., 2014). A systematic analysis for the similarity between the yield and LAI estimation is essential for the yield prediction. Therefore, in this study, MS images and digital images at critical growth stages were acquired and VIs were correlated to the grain yield and LAI to (1) determine the best period and optimal VIs for rice grain yield prediction; (2) assess the potential of multi-temporal VIs for grain yield prediction based on UAV images.

2. Material and methods

2.1. Experimental design

The study was conducted at the experiment station of the National Engineering and Technology Center for Information Agriculture (NETCIA), which is located in Rugao city, Jiangsu province, China (120°45′E, 32°16′N). The predominant soil type is loam and the organic carbon concentration in the soil is 12.95 $g \cdot kg^{-1}$. The annual average temperature, number of precipitation days, and precipitation are 14.6 °C, 121.3, and 1055.5 mm, respectively. Two field-plot experiments involving different rice (*Oryza sativa L.*) cultivars, nitrogen application rates, planting densities were designed for this study, as summarized in Table 1. And three rice cultivars with different plant types were selected in this study including two *indica* rice cultivars: Y liangyou 1 (compact plant type with erect leaf), Liangyou 728 (semi-compact plant type) and one *japonica* rice cultivar: Wuyunjing 24 (loose plant type with inclined leaf).

Experiment 1 (Exp. 1): The experiment was conducted for a single season from June 2015 to November 2015. Two rice cultivars (Wuyunjing 24 and Y liangyou 1) were sown on 16 May and transplanted on 15 June with two planting densities. The plot areas were 30 m^2 (6 m length × 5 m width). Four N fertilization rates were applied in the form of urea at the rate of 40% at preplanting, 20% at tillering, 20% at jointing, and 20% at booting. In addition, 135 $kg \cdot ha^{-1}$ P_2O_5 as a phosphate fertilizer supplement and 190 $kg \cdot ha^{-1}$ K_2O as potash fertilizer were applied in all the experimental plots. Every treatment had three replications and a total of 36 plots (12 treatments) within a randomized complete block design were grown for the whole study.

Experiment 2 (Exp. 2): The experiment was conducted for a single season from June 2015 to November 2015. Two rice cultivars were sown on 16 May and transplanted on 15 June at three planting densities. The plot areas were 30 m^2 with 6 m length and 5 m width. Two N fertilization rates were applied in the form of urea at the rate of 40% at preplanting, 20% at tillering, 20% at jointing, and 20% at booting. Every treatment had three replications with a total of 36 plots (12 treatments) within a randomized complete block design grown for the whole study. Phosphate and potassium fertilizers were applied as described for Exp. 1.

In these experiments, N levels were determined based on the growth status of rice and the weather conditions during various growth stages. Management practices during the experiment were based on local production standards.

2.2. Field data collection

Repeated destructive sampling was carried out in each plot for Exp. 1 and Exp. 2. After the UAV flight, three hills from each experimental plot were randomly selected to determine LAI. For each sample, the green leaves were separated from the stems and immediately scanned using the Laser area meter (LI-3100C; LI-COR Inc., NE, USA). The leaf area was then obtained and the LAI for each plot was calculated based on the planting densities. At maturity, 30 hills from each plot were harvested manually for

Table 1
Experimental design of the two UAV remote sensing experiments conducted in 2015.

Experiment	Date (y/m)	Cultivars	Plant density (cm × cm)	Nitrogen application rate (kg·ha^{-1})
1	2015/6–2015/10	Wuyunjing 24	30 × 15	0
		Y liangyou 1	50 × 15	100
				200
				300
2	2015/6–2015/10	Wuyunjing 24	30 × 15	100
		Liangyou 728	40 × 15	300
			20 × 15	

calculation of grain yield. The seeds were dried under sunlight, and the grain yield was determined.

2.3. UAV, sensor and image acquisition

The UAV used in this study is a multi-rotor MK-Oktokopter manufactured by HiSystems GmbH (Fig. 1). The maximum payload capacity is 2.5 kg, and the maximum flight range is 1000 m. The flight duration varies between 8 and 25 min depending on the battery and payload. A digital camera (EOS 5D Mark III; Canon, Inc., Tokyo, Japan) and a six-band multispectral camera (Mini-MCA6; Tetracam, Inc., Chatsworth, CA, USA) were mounted on the UAV to allow us to acquire digital and MS images (Garcia-Ruiz et al., 2013; Del Pozo et al., 2014; Herrero-Huerta et al., 2014). The band selected for this study is comprised of center wavelengths of 490, 550, 680, 720, 800, and 900 nm. The camera specifications are listed in Table 3.

The UAV campaign was conducted under clear skies and low wind speed conditions between 10:00 and 14:00 local time. The MK-Tool autopilot was used to set the flight waypoints. The altitudes for acquisition of MS images and RGB images were 100 m and 50 m, respectively. Camera settings were adjusted according to the lighting conditions and set to a fixed exposure for each flight. The images were acquired continuously during the flight at 0.5 Hz and saved to memory cards. The details of the images acquired are shown in Table 2.

2.4. Image processing

The Mini-MCA MS camera consists of six individual channels, and the processing workflow for the MS images includes noise correction, vignetting correction, lens distortion correction, band-to-band registration, band stacking, and radiometric calibration (Laliberte et al., 2011; Kelcey and Lucieer, 2012; Del Pozo et al., 2014). All processing was performed using the IDL script within the ENVI software package (EXELIS; Boulder, CO, USA). One hundred dark offset sample images were generated for each of the six Mini-MCA channels at multiple exposure levels. The per-pixel average was calculated for each combination of sensor and exposure levels and stored as a noise correction file. Lens vignetting correction was based on spatially dependent correction factors. The correction factors for each sensor at multiple exposure levels were generated from the average of 100 flat field sample images with the uniform source system (CSTM-USS-1200C; Labsphere, Inc., New England, USA). A Brown-Conrady distortion model was adopted for lens distortion. Since the Mini-MCA6 has a significant band mis-registration effect, GCPs were used for band-to-band registration. Six images were then stacked into a 6-band image for further analysis. For radiometric calibration, seven calibration targets (1.2 m × 1.2 m) with nominal reflectance of 3%, 6%, 12%, 22%, 48%, 64%, and 80% were placed within the UAV flight path and captured in the mini-MCA imagery. The target's actual digital number (DN) values were extracted from the airborne image and the reflectance measured with a FieldSpec 4 Spectroradiometer (Analytical Spectral Devices; Boulder, CO USA). The DNs in the raw images were then transformed into the ground measured reflectance data by applying an empirical linear correction method. The preprocessing of the digital images includes lens distortion correction and mosaicking. Image mosaicking was conducted with PhotoScan Professional software (Agisoft LLC, ST. Petersburg, Russia).

2.5. Model establishment/data analysis

A large number of vegetation indices have been proposed for leaf area index (LAI) estimation and grain yield prediction. Seven types of spectral indices and six color indices were chosen for

Fig. 1. Illustration of the UAV calibration system.

Table 2
Acquisition of multispectral (MS) images and digital images for the two experiments.

Experiment	MS images		Digital images	
	Acquisition date (y/m/d)	Growth stage	Acquisition date (y/m/d)	Growth stage
1	2015/07/09	Initial tillering	2015/07/13	Initial tillering
	2015/07/21	Tillering	2015/07/21	Tillering
	2015/07/28	Jointing	2015/07/28	Jointing
	2015/08/15	Initial booting	2015/08/14	Initial booting
	2015/08/25	Booting	2015/08/25	Booting
	2015/09/09	Heading	2015/09/10	Heading
	2015/09/27	Filling	2015/09/27	Filling
2	2015/07/13	Initial tillering	2015/07/13	Initial tillering
	2015/07/21	Tillering	2015/07/21	Tillering
	2015/07/28	Jointing	2015/07/28	Jointing
	2015/08/12	Initial booting	2015/08/14	Initial booting
	2015/08/25	Booting	2015/08/25	Booting
	2015/09/09	Heading	2015/09/10	Heading
	2015/09/24	Filling	2015/09/27	Filling

Table 3
Basic parameters for the two cameras mounted on the UAV.

Sensor	Spectral band (nm)	Resolution (pixels)	Weight (g)	Ground resolution at 100 m high (cm)
Mini-MCA6	490, 550, 680, 720, 800, 900	1280 × 1024	700	5.4
Canon EOS 5D Mark III	R, G, B	5760 × 3840	1230	3.0

Table 4
Equations for spectral indices and color indices used in this study.

		Algorithm formula	Reference
Vegetation index	RVI (λ1,λ2)	$R_{\lambda1}/R_{\lambda2}$	Jordan (1969)
	DVI(λ1,λ2)	$R_{\lambda1}-R_{\lambda2}$	Jordan (1969)
	NDVI (λ1,λ2)	$(R_{\lambda1}-R_{\lambda2})/(R_{\lambda1}+R_{\lambda2})$	Rouse (1974)
	MTVI2	$1.5(1.2(R_{800}-R_{550})-2.5(R_{670}-R_{550}))/(2(R_{800}+1)^2-(6R_{800}-5(R_{670})^{0.5}-0.5)^{0.5}$	Haboudane et al. (2004)
	SAVI	$1.5(R_{870}-R_{680})/(R_{870}+R_{680}+0.5)$	Huete (1988)
	RDVI	$(R_{800}-R_{670})/(R_{800}+R_{670})^{0.5}$	Roujean and Breon (1995)
	EVI	$2.5(R_{NIR}-R_{680})/(1+R_{NIR}+6R_{680}-7.5R_{475})$	Huete et al. (1994)
Color index	NDI	(g−r)/(g+r)	Woebbecke et al. (1995)
	ExG	2g-r-b	Woebbecke et al. (1995)
	ExR	1.4r-g	Meyer and Neto (2008)
	ExGR	3g-2.4r-b	Meyer and Neto (2008)
	VARI	(g−r)/(g+r−b)	Gitelson et al. (2002)
	GLI	(2g−b−r)/(2g+b+r)	Louhaichi et al. (2001)

the MS images and RGB images, respectively (Table 4). The spectral index was calculated with reflectance derived from MS image, while the color index was calculated with normalized DNs (Saberioon et al., 2014; Torres-Sanchez et al., 2015). The following normalization scheme was applied to the color index:

$$r = R/(R+G+B); g = G/(R+G+B); b = B/(R+G+B) \quad (1)$$

where R, G and B are the DNs of the red, green and blue bands, respectively.

Five types of mathematical functions were used to analyze the relationship between grain yield, LAI and VIs including linear function, exponential function, logarithmic function, polynomial function, and power function. Correlation coefficients (R^2) and root-mean-square error (RMSE) were computed with MATLAB 7.10 (MathWorks; Inc. Natick, Massachusetts, USA) and used to assess the performance of the estimation models.

In addition to the analysis between the grain yield and VIs at single growth stage, the multi-temporal VIs was also analyzed. Previous studies have shown that the multi-temporal VIs can improve the prediction accuracy for the grain yield. In this study, three forms of multi-temporal VIs were calculated: VIs at two random growth stages investigated with the multiple linear regression function [MLR(VI)] (Eq. (2)), the sum of VIs at two random growth stages [SUM(VI)] (Eq. (3)) and the accumulative VI ($\sum$VI), which is defined as the enclosed area of the zone by growth processes and the dynamic curve of VI with day after transplanting (Eq. (4)).

$$\mathrm{MLR(VI)} = a \times x_i + b \times x_j + c \quad (2)$$

$$\mathrm{SUM(VI)} = x_i + x_j \quad (3)$$

$$\sum \mathrm{VI} = \int_m^n \mathrm{VI}\, dt = \sum_{i=m}^{n} \frac{1}{2}(x_i + x_{i+1}) \quad (4)$$

where x_i, x_j represent the VI values at two different growth stages, and m, n represent the days after transplanting (DAT) for the two growth stages.

3. Results

3.1. Rice grain yield and LAI estimation with spectral/color index at a single stage

3.1.1. Relationship between rice LAI and spectral/color index

LAI is an important parameter that indicates crop photosynthesis and growth status and is of significance for crop yield prediction

(Noureldin et al., 2013; Verger et al., 2014). The relationships between LAI and the spectral indices at different growth stages were analyzed (Table 5). The results showed that spectral indices were significantly correlated with LAI in the early and middle growth stages. EVI, RDVI, $NDVI_{[800,680]}$, and SAVI were obviously saturated due to the high LAI values at booting, while $DVI_{[800,720]}$, $RVI_{[800,720]}$, and $NDVI_{[800,720]}$ performed well which composed of the red edge band (720 nm) and near infrared band (800 nm). $DVI_{[800,720]}$ performed the best over the entire growth period with R^2 of 0.79 (Fig. 2a).

Similarly, the relationship between the color index and LAI was also analyzed (Table 5). Color indices performed well in the early growth stages, and VARI performed the best from initial tillering to the booting stage (Fig. 2b). VARI, NDI, and ExR showed better performances at booting, while the other color indices saturated severely. The correlation between color index and LAI decreased significantly after the heading stage. Thus, the LAI estimation model (Initial tillering to booting stage) was developed based on VARI derived from the digital images (R^2 = 0.77).

3.1.2. Relationship between rice grain yield and spectral/color index

The relationships between rice grain yield and the six spectral indices at different growth stages were analyzed using the datasets (Table 6). The results showed a good linear correlation between grain yield and all spectral indices during the jointing stage, the initial booting stage, and the booting stage. While most of the spectral indices showed a lower correlation with grain yield at the tillering and filling stages, five spectral indices at the booting stage performed best. Similar to the LAI estimation, VIs: $NDVI_{[800,720]}$ and $RVI_{[800,720]}$ composed of the red edge band and the Nir-red band gave much higher correlations with grain yield, and the maximum value of the determination coefficient was 0.75 for $NDVI_{[800,720]}$ at the booting stage. Thus, grain yield can be estimated with $NDVI_{[800,720]}$ at the booting stage (RMSE = 947.69 kg·ha^{-1}) (Fig. 3a).

The color index of the digital images showed a logarithmic relationship with grain yield. The booting stage was also the best stage for yield prediction based on the color index, and the correlation between grain yield and color index decreased markedly after heading (Table 6). The color indices (VARI, NDI, and EXR) showed high correlations with grain yield, and the VARI performed the best (R^2 = 0.70, RMSE = 1020.14 kg·ha^{-1}) (Fig. 3b).

And the VIs: VARI and $NDVI_{[800,720]}$ showed high correlation with the high value LAI were performed well for yield prediction. Especially, the VIs composed of the red edge band and the Nir-red band showed a high potential for grain yield and LAI estimation.

3.2. Grain yield estimation with multi-temporal spectral/color indices

3.2.1. Relationships between grain yield and multi-temporal spectral indices

Based on the results from Section 3.1, further analysis was conducted on the relationships between grain yield and

Table 5
Correlations between LAI and vegetation indices at different growth stages in rice.

Growth stage	Spectral index									Color index					
	EVI	RDVI	$RVI_{[800,550]}$	$RVI_{[800,720]}$	$DVI_{[800,720]}$	$NDVI_{[800,680]}$	SAVI	MTVI2	$NDVI_{[800,720]}$	ExG	GLI	VARI	NDI	ExR	ExG-ExR
Initial booting	0.53	0.62	0.88	0.86	0.80	0.67	0.61	0.59	0.89	0.37	0.38	0.72	0.66	0.67	0.49
Booting	0.44	0.49	0.75	0.76	0.62	0.55	0.49	0.47	0.78	0.21	0.21	0.57	0.50	0.51	0.33
Heading	0.57	0.56	0.26	0.49	0.67	0.34	0.61	0.63	0.42	0.09	0.07	0.23	0.18	0.16	0.09
Tillering - booting	0.64	0.69	0.79	0.84	0.80	0.63	0.69	0.59	0.80	0.58	0.58	0.77	0.74	0.74	0.65
Whole growth period	0.66	0.69	0.69	0.69	0.79	0.63	0.69	0.58	0.70	0.37	0.38	0.36	0.36	0.33	0.41

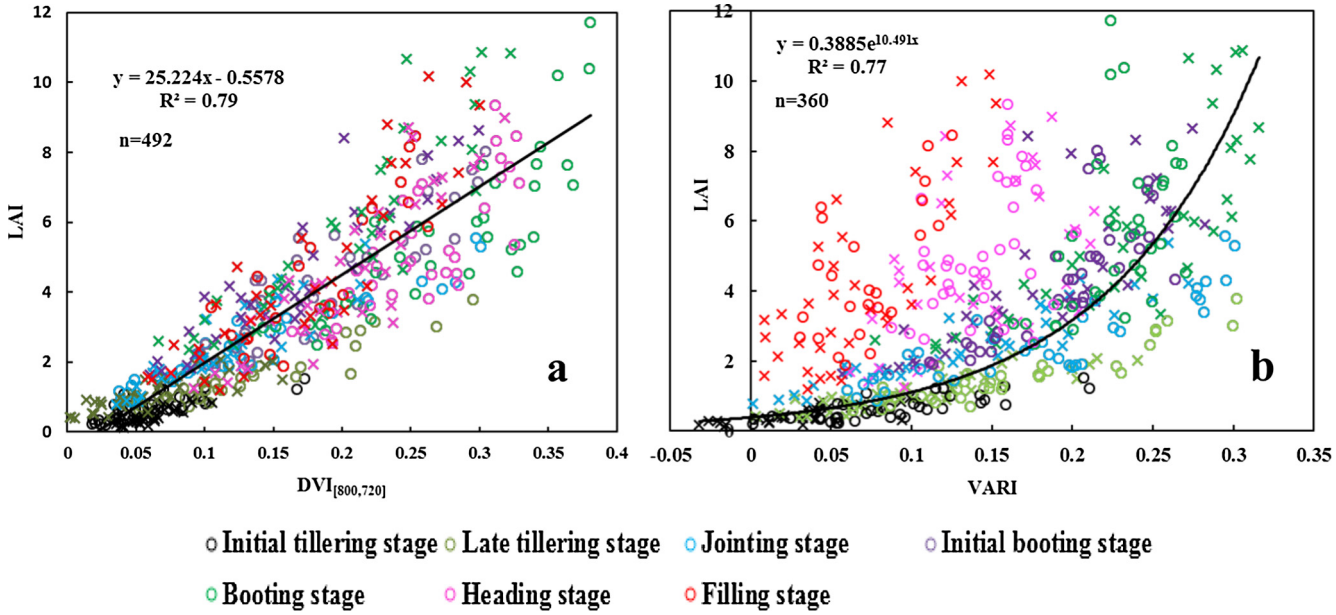

Fig. 2. Relationship between LAI and $DVI_{[800,\ 720]}$ (Initial tillering to filling stage) (a) and VARI (Initial tillering to booting stage) (b) in rice.

Table 6
Correlations between grain yield and vegetation indices at different growth stages in rice.

Growth stage	Spectral index						Color index					
	$NDVI_{[800,680]}$	$DVI_{[800,720]}$	$RVI_{[800,550]}$	$RVI_{[800,680]}$	$NDVI_{[800,720]}$	$RVI_{[800,720]}$	ExG	GLI	VARI	NDI	ExR	ExG-ExR
Initial tillering	0.44	0.28	0.36	0.21	0.54	0.31	0.18	0.19	0.28	0.26	0.26	0.21
Tillering	0.49	0.36	0.42	0.21	0.61	0.49	0.29	0.30	0.44	0.40	0.39	0.33
Jointing	0.61	0.42	0.48	0.31	0.47	0.46	0.42	0.43	0.53	0.50	0.49	0.45
Initial booting	0.65	0.57	0.51	0.42	0.64	0.57	0.33	0.35	0.62	0.56	0.55	0.43
Booting	0.66	0.50	0.64	0.49	0.75	0.67	0.26	0.27	0.71	0.59	0.58	0.40
Heading	0.40	0.54	0.31	0.21	0.61	0.53	0.12	0.13	0.34	0.28	0.27	0.17
Filling	0.43	0.64	0.49	0.40	0.59	0.55	0.14	0.14	0.37	0.33	0.33	0.25

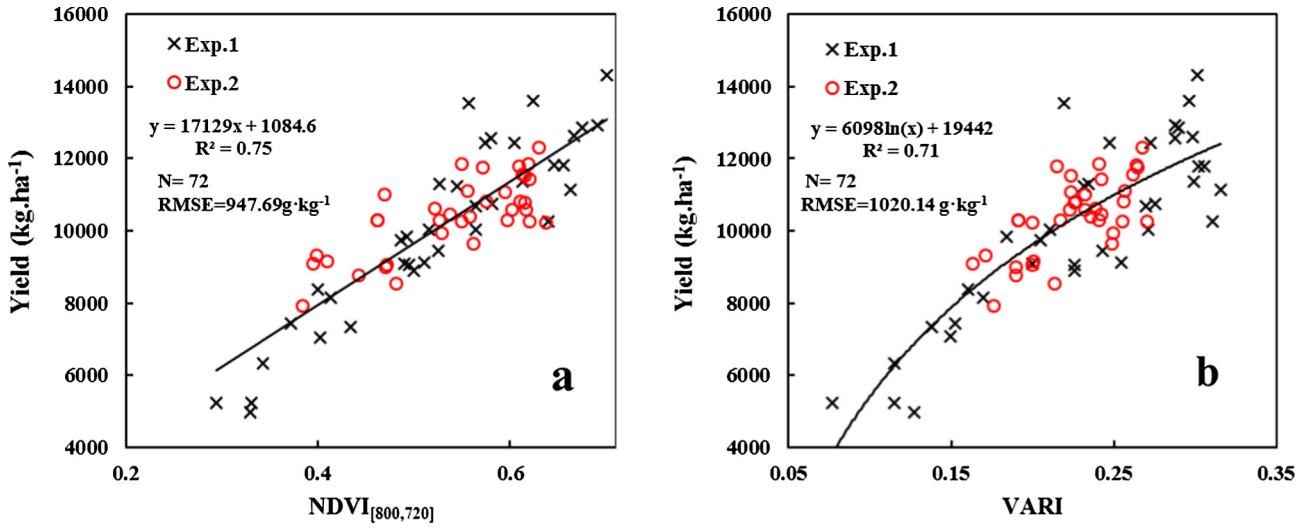

Fig. 3. Relationships between grain yield and spectral index $NDVI_{[800,720]}$ (a), and color index VARI (b) in rice.

multi-temporal spectral indices (Fig. 4). Initially, $NDVI_{[800,720]}$ at two random growth stages were investigated with the multiple linear regression: MLR($NDVI_{[800,720]}$) (Fig. 3a). The results showed that MLR($NDVI_{[800,720]}$) combining VIs at the booting stage with another growth stage gave a better correlation with grain yield than did VI at a single growth stage (Fig. 4a). Comparably, the optimal fit was found for the MLR model with combinations of booting stage and heading stage (R^2 = 0.76, RMSE = 926.46 kg·ha^{-1}) (Eq. (5); Fig. 5a). In addition, the relationship between grain yield and SUM($NDVI_{[800,720]}$) was also studied (Fig. 4b), and VIs combining booting stage with heading stage performed best with R^2 of 0.75 (Fig. 5b).

$$\text{Yield} = 13980.29 \times NDVI_{[800,720](\text{Booting})} + 5798.10 \times NDVI_{[800,720](\text{Heading})} + 115.15 \quad (5)$$

where $NDVI_{[800,720](\text{Booting})}$, $NDVI_{[800,720](\text{Heading})}$ represent the $NDVI_{[800,720]}$ values at booting stage and heading stage.

The accumulative VI:$\sum NDVI_{[800,720]}$, was correlated to rice grain yield (Fig. 4c). The result showed that the correlation between grain yield and $\sum NDVI_{[800,720]}$ increased as the $NDVI_{[800,720]}$ accumulated with growth stages. $\sum NDVI_{[800,720]}$ from booting to the heading stage performed the best (R^2 = 0.75). Thus, the best period for grain yield prediction is from the booting stage to the heading stage.

3.2.2. Relationships between grain yield and multi-temporal color indices

The correlation between the multi-temporal color indices and rice grain yield was also analyzed. Fig. 4d shows the relationship between rice grain yield and MLR(VARI) at two random growth stages. The combined VIs from two stages including the booting stage gave a higher correlation than did the VI from a single growth stage. An optimal fit was found for MLR model combinations of VIs at the jointing and booting stages with R^2 of 0.73 and RMSE of 987.02 kg·ha^{-1} (Eq. (6); Fig. 5d). Similar results were achieved for the quantitative analysis of the relationship between grain yield and SUM(VARI). The booting stage combined with one other stage showed a higher correlation with grain yield (Fig. 4e). SUM(VARI) combing VIs at booting and the initial booting stage performed best with R^2 of 0.72 (Fig. 5e).

$$\text{Yield} = 7100 \times VARI_{(\text{Jointing})} + 23197 \times VARI_{[800,720](\text{Booting})} + 3853 \quad (6)$$

where $VARI_{(\text{Jointing})}$, $VARI_{(\text{Booting})}$ represent the VARI values at jointing stage and booting stage.

The relationships between rice grain yield and $\sum$VARI was analyzed (Fig. 4f). The results showed that the correlation between grain yield and $\sum$VARI increased as the VARI accumulated before the heading stage, while it decreased as the VARI accumulated to the heading stage and filling stage. The best performance was obtained with $\sum$VARI from the initial booting stage to the booting stage with R^2 values of 0.72 (Fig. 5f).

4. Discussion

At present, the ability to rapidly predict crop yields in real time based on RS data is an area of active research. There have been preliminary applications of VIs, such as NDVI and EVI2, in grain yield prediction in wheat (Reyniers et al., 2006), barley (Mkhabela et al., 2011), maize, and soybean (Bolton and Friedl, 2013). Zhao et al.

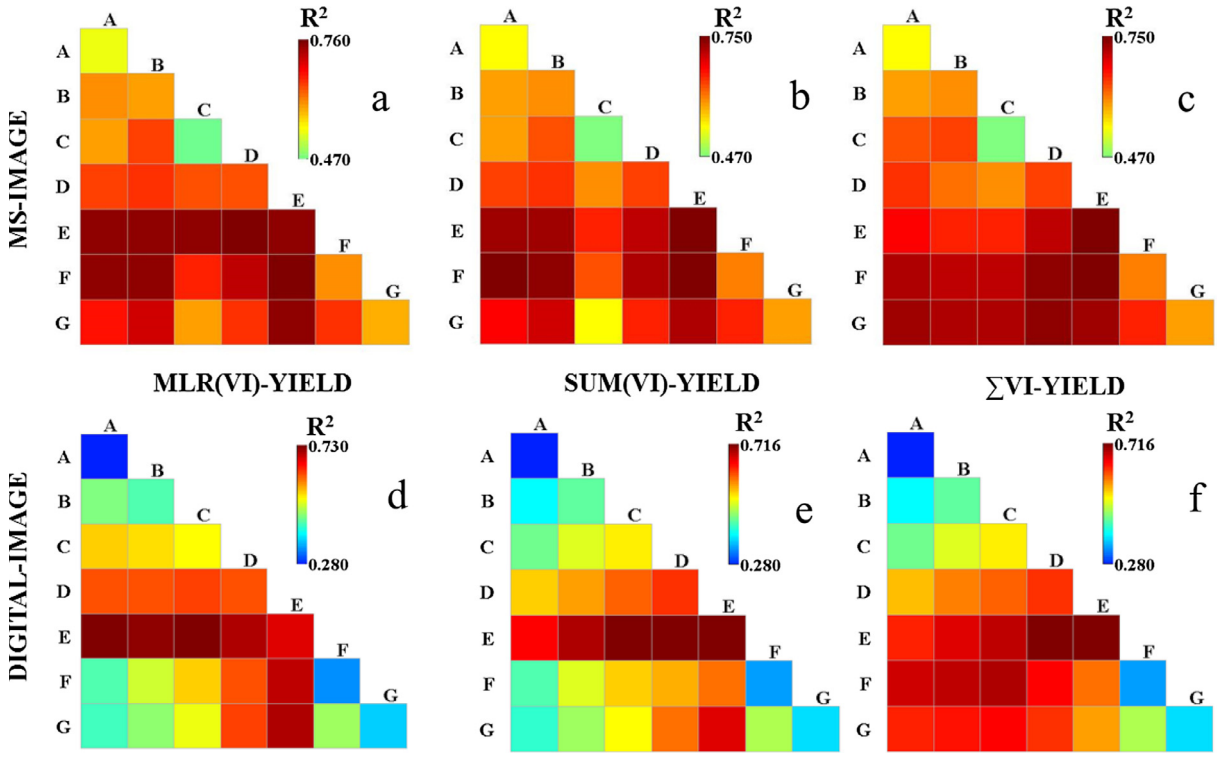

A: Initial tillering; B: Late tillering; C: Jointing; D: Initial booting; E: Booting; F: Heading; G: Filling

Fig. 4. Correlations of grain yields to $NDVI_{[800,720]}$ (a), and VARI (d) at two growth stages based on multiple linear regression; the sum of VIs at two growth stages: $NDVI_{[800,720]}$ (b), and VARI (e); the cumulative vegetation indices: $\sum NDVI_{[800,720]}$ (c), and $\sum$VARI (f).

(2007) predicted cotton yield using different VIs and found that RVI showed good prediction accuracy. However, there are few reports describing crop yield estimation based on the UAV system. In this study, the relationships between rice grain yield and the color index from digital images and the spectral indices from MS images were studied at different growth stages based on images taken by a UAV. Results showed that the color indices and spectral indices of the jointing stage, initial booting stage, and the booting stage had higher correlations with rice grain yield, and the booting stage gave the highest correlation. Previously published results indicated that the booting stage could provide higher prediction accuracy when using RS to predict wheat yield (Xue et al., 2007), and Chang et al. (2005) also successfully predicted rice yield using reflectance measured at booting stage, which is consistent with the results from this study. Thus, the booting stage may be the best period and the boundary point for the estimation of grain yield in rice.

The booting stage represents the nutrient growth peak of the rice plant and has the highest LAI, which can well reflect the maximal photosynthetic capacity and yield potential. Becker-Reshef et al. (2010) successfully estimated wheat yield using the NDVI value when the LAI reached its maximum. VIs become saturated easily in later growth stages due to the high level of vegetation coverage (Gitelson et al., 2002). Therefore, choosing an appropriate VI and avoiding the saturation problem in LAI estimation is very important for the accurate prediction of rice grain yield. DVI, NDVI, and RVI composed of red edge band (720 nm) and near infrared band (800 nm) were found to be effective in predicting rice LAI and yield in this study, which is consistent with the results of Verger et al. (2014). In the later growth stages, the appearance of the rice panicle and the increase in yellow leaves enhances the difficulty of LAI estimation and yield prediction. We found that the spectral indices $RVI_{[800,550]}$ and $RVI_{[800,720]}$, and the color indices NDI, ExG, and VARI performed well in LAI estimation and yield prediction in the early growth stages, but their correlation with LAI and yield was lower after the heading stage. Sakamoto et al. (2011) also found that the color index VARI performed well before the booting stage but poorly in the late growth stages.

Some studies have indicated that the accumulative VI can improve the stability of yield prediction (Serrano et al., 2000; Wang et al., 2014). Our results in rice confirmed this, and strongly indicate that the booting stage is a critical period for rice grain yield estimation. Adding one or more growth stages based on the booting stage can improve the estimation accuracy. The correlation between grain yield and VARI (booting stage) increased from 0.70 to 0.73 and RMSE decreased from 1020.14 to 987.02 $kg \cdot ha^{-1}$ when the VARI (jointing stage) was added with MLR model. Similar results was obtained when $NDVI_{[800,720]}$ at heading stage was added to the $NDVI_{[800,720]}$ at booting stage with R^2 increased from 0.75 to 0.76 and RMSE decrease from 947.69 to 926.46 $kg \cdot ha^{-1}$. The biomass and LAI at booting stage showed high correlation with grain yield, while the total growth index over a period time can better track the process of yield formation (Xue et al., 2005). Ren et al. (2008) also obtained similar results that $\sum$NDVI from booting to the flowering stage exhibited better performance than a single stage did in wheat grain yield prediction.

The potential of MS and digital images for LAI estimation and yield prediction has been compared systematically. Digital cameras are cost effective, convenient to use, and simple to operated sensors with ultra-high resolution (Bendig et al., 2015). The multi-

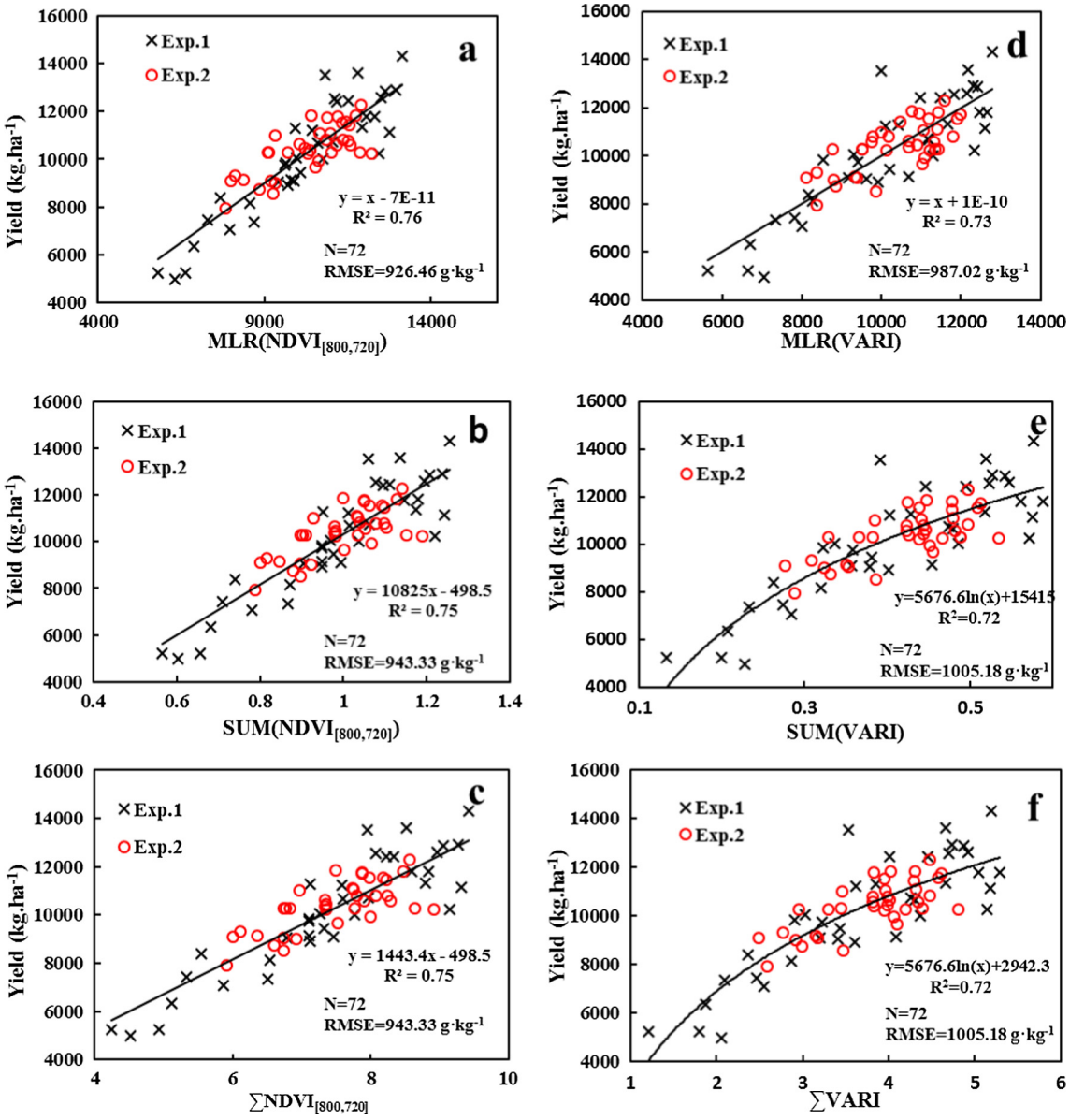

Fig. 5. Relationship between grain yield and multi-temporal VIs: MLR($NDVI_{[800,720]}$) at the booting and heading stages (a); SUM($NDVI_{[800,720]}$) (b), and $\sum NDVI_{[800,720]}$ (c) at the booting and heading stages; and MLR(VARI) at the jointing and booting stages (d); SUM(VARI) (e), and ∑VARI(f) at the initial booting and booting stages.

spectral sensor (Mini-MCA) is a high cost sensor with a geometric resolution of 1280 × 1024 pixels. And MS image processing is relatively more complex than is digital image processing (Garcia-Ruiz et al., 2013; Laliberte et al., 2011). It is convenient to randomly choose the most suitable band combinations and then integrate them within a sensor based on the requirements of study (Verger et al., 2014; Zhang and Kovacs, 2012). In this study, the spectral indices derived from the MS images correlated better with LAI and grain yield than did the color indices during the whole growth period. The spectral indices $DVI_{[800,720]}$, $RVI_{[800,720]}$, and $NDVI_{[800,720]}$ composed of the red edge band and Nir-red band can relieve the saturation phenomenon in estimating LAI at the booting stage. In addition, these indices overcome the negative effect caused by rice panicles during the late growth stages of rice. However, the color indices derived from the digital images were highly correlated with the LAI and grain yield early in the growth season, but the correlation was poor after the heading stage. Therefore, the early and middle growth stages (jointing to booting) are suitable for rice grain yield estimation based on digital image. While a combination of the early to later stages (especially booting to heading) can obtain a higher yield prediction accuracy for the MS images.

5. Conclusion

UAVs have become a new platform for acquiring high spatio-temporal resolution images used for precision agriculture. The single stage VI and multi-temporal VIs were explored for grain yield prediction in rice based on MS images and digital images from UAV. This study has demonstrated that both MS and digital images acquired are reliable for rice growth and grain yield estimation.

The booting stage was identified as the best growth stage for grain yield estimating with VI from a single stage for both MS and digital images. The corresponding optimal VIs were $NDVI_{[800,720]}$ and VARI. The VIs that showed a high correlation with LAI performed well for yield prediction. Especially, the VIs composed of red edge band (720 nm) and near infrared band

(800 nm) were found to be more effective in predicting yield and LAI at high level.

The prediction accuracy was found to increase when another growth stage was added based on the booting stage. For instance, MLR($NDVI_{[800,720]}$) at the booting and heading stages, and MLR (VARI) at the booting and jointing stages performed better than did a single growth stage.

The spectral index (MS image) showed higher correlation with the grain yield and LAI than did the color index (digital image). However, the digital camera as a cost effective sensor is reliable for rice growth monitoring before the heading stage.

The yield estimation models and method should be further examined with multi-year datasets. In addition, yield-related agronomic parameters such as LAI and crop growth period can be further analyzed and integrated into the models to improve crop grain yield prediction accuracy.

Acknowledgements

This research was supported by the National High Technology Research and Development Program of China (863 Program) (2013AA102301), the National Natural Science Foundation of China (31371535), the Jiangsu Distinguished Professor Program, the Jiangsu Collaborative Innovation Center for Modern Crop Production, and the Priority Academic Program Development of Jiangsu Higher Education Institutions (PAPD).

References

Becker-Reshef, I., Vermote, E., Lindeman, M., Justice, C., 2010. A generalized regression-based model for forecasting winter wheat yields in Kansas and Ukraine using MODIS data. Remote Sens. Environ. 114, 1312–1323.
Bendig, J., Bolten, A., Bennertz, S., Broscheit, J., Eichfuss, S., Bareth, G., 2014. Estimating biomass of barley using crop surface models (csms) derived from uav-based rgb imaging. Remote Sens. 6 (11), 10395–10412.
Bendig, J., Yu, K., Aasen, H., Bolten, A., Bennertz, S., Broscheit, J., Gnyp, M.L., Bareth, G., 2015. Combining UAV-based plant height from crop surface models, visible, and near infrared vegetation indices for biomass monitoring in barley. Int. J. Appl. Earth Obs. Geoinf. 39, 79–87.
Bolton, D.K., Friedl, M.A., 2013. Forecasting crop yield using remotely sensed vegetation indices and crop phenology metrics. Agric. For. Meteorol. 173, 74–84.
Chang, K.W., Shen, Y., Lo, J.C., 2005. Predicting rice yield using canopy reflectance measured at booting stage. Agron. J. 97 (3), 872–878.
Córcoles, J.I., Ortega, J.F., Hernández, D., Moreno, M.A., 2013. Estimation of leaf area index in onion (Allium cepa L.) using an unmanned aerial vehicle. Biosyst. Eng. 115, 31–42.
Del Pozo, S., Rodriguez-Gonzalvez, P., Hernandez-Lopez, D., Felipe-Garcia, B., 2014. Vicarious radiometric calibration of a multispectral camera on board an unmanned aerial system. Remote Sens. 6, 1918–1937.
Fu, Y., Yang, G., Wang, J., Song, X., Feng, H., 2014. Winter wheat biomass estimation based on spectral indices, band depth analysis and partial least squares regression using hyperspectral measurements. Comput. Electron. Agric. 100, 51–59.
Garcia-Ruiz, F., Sankaran, S., Maja, J.M., Lee, W.S., Rasmussen, J., Ehsani, R., 2013. Comparison of two aerial imaging platforms for identification of Huanglongbing-infected citrus trees. Comput. Electron. Agric. 91, 106–115.
Geipel, J., Link, J., Claupein, W., 2014. Combined spectral and spatial modeling of corn yield based on aerial images and crop surface models acquired with an unmanned aircraft system. Remote Sens. 6 (11), 10335–10355.
Gitelson, A.A., Kaufman, Y.J., Stark, R., Rundquist, D., 2002. Novel algorithms for remote estimation of vegetation fraction. Remote Sens. Environ. 80, 76–87.
Haboudane, D., Miller, J.R., Pattey, E., Zarco-Tejada, P.J., Strachan, I.B., 2004. Hyperspectral vegetation indices and novel algorithms for predicting green LAI of crop canopies: Modeling and validation in the context of precision agriculture. Remote Sens. Environ. 90, 337–352.
Haboudane, D., Miller, J.R., Tremblay, N., Zarco-Tejada, P.J., Dextraze, L., 2002. Integrated narrow-band vegetation indices for prediction of crop chlorophyll content for application to precision agriculture. Remote Sens. Environ. 81, 416–426.
Hamar, D., Ferencz, C., Lichtenberger, J., Ferencz-Árkos, G.T.I., 1996. Yield estimation for corn and wheat in the Hungarian Great Plain using Landsat MSS data. Int. J. Remote Sens. 17, 1689–1699.
Herrero-Huerta, M., Hernandez-Lopez, D., Rodriguez-Gonzalvez, P., Gonzalez-Aguilera, D., Gonzalez-Piqueras, J., 2014. Vicarious radiometric calibration of a multispectral sensor from an aerial trike applied to precision agriculture. Comput. Electron. Agric. 108, 28–38.
Huete, A.R., 1988. A Soil-Adjusted Vegetation Index (SAVI). Remote Sens. Environ. 25 (3), 295–309.
Huete, A., Justice, C., Liu, H., 1994. Development of vegetation and soil indexes for MODIS-EOS. Remote Sens. Environ. 49 (3), 224–234.
Hunt, E.R.J., Cavigelli, M., Daughtry, C.S.T., McMurtrey, J.I., Walthall, C.L., 2005. Evaluation of digital photography from model aircraft for remote sensing of crop biomass and nitrogen status. Precision Agric. 6, 359–378.
Jannoura, R., Brinkmann, K., Uteau, D., Bruns, C., Joergensen, R.G., 2015. Monitoring of crop biomass using true colour aerial photographs taken from a remote controlled hexacopter. Biosyst. Eng. 129, 341–351.
Jordan, C.F., 1969. Derivation of leaf area index from quality of light on the forest floor. Ecology 50 (4), 663–666.
Kelcey, J., Lucieer, A., 2012. Sensor correction of a 6-band multispectral imaging sensor for UAV remote sensing. Remote Sens. 4, 1462–1493.
Laliberte, A.S., Goforth, M.A., Steele, C.M., Rango, A., 2011. Multispectral remote sensing from unmanned aircraft: image processing workflows and applications for rangeland environments. Remote Sens. 3, 2529–2551.
Li, X., Lee, W.S., Li, M., Ehsani, R., Mishra, A.R., Yang, C., Mangan, R.L., 2012. Spectral difference analysis and airborne imaging classification for citrus greening infected trees. Comput. Electron. Agric. 83, 32–46.
Liang, L., Di, L., Zhang, L., Deng, M., Qin, Z., Zhao, S., Lin, H., 2015. Estimation of crop LAI using hyperspectral vegetation indices and a hybrid inversion method. Remote Sens. Environ. 165, 123–134.
Liang, S., 2004. Quantitative Remote Sensing of Land Surfaces. Wiley-Interscience, USA, DC.
Louhaichi, M., Borman, M.M., Johnson, D.E., 2001. Spatially located platform and aerial photography for documentation of grazing impacts on wheat. Geocarto International 16 (1), 65–70.
Meyer, G.E., Neto, J.O.C., 2008. Verification of color vegetation indices for automated crop imaging applications. Comput. Electron. Agric. 63 (2), 282–293.
Mkhabela, M.S., Bullock, P., Raj, S., Wang, S., Yang, Y., 2011. Crop yield forecasting on the Canadian Prairies using MODIS NDVI data. Agric. For. Meteorol. 151, 385–393.
Moran, M.S., Inoue, Y., Barnes, E.M., 1997. Opportunities and limitations for image-based remote sensing in precision crop management. Remote Sens. Environ. 61, 319–346.
Noureldin, N.A., Aboelghar, M.A., Saudy, H.S., Ali, A.M., 2013. Rice yield forecasting models using satellite imagery in Egypt. Egypt. J. Remote Sens. Space Sci. 16, 125–131.
Panda, S.S., Ames, D.P., Panigrahi, S., 2010. Application of vegetation indices for agricultural crop yield prediction using neural network techniques. Remote Sens. 2, 673–696.
Pradhan, S., Bandyopadhyay, K.K., Sahoo, R.N., Sehgal, V.K., Singh, R., Gupta, V.K., Joshi, D.K., 2014. Predicting wheat grain and biomass yield using canopy reflectance of booting stage. J. Indian Soc. Remote Sens. 42, 711–718.
Ren, J., Chen, Z., Zhou, Q., Tang, H., 2008. Regional yield estimation for winter wheat with MODIS-NDVI data in Shandong, China. Int. J. Appl. Earth Obs. Geoinf. 10, 403–413.
Reyniers, M., Vrindts, E., De Baerdemaeker, J., 2006. Comparison of an aerial-based system and an on the ground continuous measuring device to predict yield of winter wheat. Eur. J. Agron. 24, 87–94.
Reynolds, C.A., Yitayew, M., Slack, D.C., Hutchinson, C.F., Huete, A., Petersen, M.S., 2000. Estimating crop yields and production by integrating the FAO Crop specific Water Balance model with real-time satellite data and ground-based ancillary data. Int. J. Remote Sens. 21, 3487–3508.
Roujean, J.L., Breon, F.M., 1995. Estimating PAR absorbed by vegetation from bidirectional reflectance measurements. Remote Sens. Environ. 51 (3), 375–384.
Rouse, J.W., 1974. Monitoring the vernal advancement and retrogradation (greenwave effect) of natural vegetation. Nasa.
Saberioon, M.M., Amin, M.S.M., Anuar, A.R., Gholizadeh, A., Wayayok, A., Khairunniza-Bejo, S., 2014. Assessment of rice leaf chlorophyll content using visible bands at different growth stages at both the leaf and canopy scale. Int. J. Appl. Earth Obs. Geoinf. 32, 35–45.
Sakamoto, T., Shibayama, M., Kimura, A., Takada, E., 2011. Assessment of digital camera-derived vegetation indices in quantitative monitoring of seasonal rice growth. ISPRS J. Photogrammetry Remote Sens. 66, 872–882.
Serrano, L., Filella, I., Penuelas, J., 2000. Remote sensing of biomass and yield of winter wheat under different nitrogen supplies. Crop Sci. 40, 723–731.
Sibley, A.M., Grassini, P., Thomas, N.E., Cassman, K.G., Lobell, D.B., 2014. Testing remote sensing approaches for assessing yield variability among maize fields. Agron. J. 106, 24–32.
Stagakis, S., González-Dugo, V., Cid, P., Guillén-Climent, M.L., Zarco-Tejada, P.J., 2012. Monitoring water stress and fruit quality in an orange orchard under regulated deficit irrigation using narrow-band structural and physiological remote sensing indices. ISPRS J. Photogrammetry Remote Sens. 71, 47–61.
Swain, K.C., Thomson, S.J., Jayasuriya, H.P.W., 2010. Adoption of an unmanned helicopter for low-altitude remote sensing to estimate yield and total biomass of a rice crop. Trans. Asabe 53 (1), 21–27.
Teoh, C.C., Nadzim, N.M., Shahmihaizan, M.J.M., Izani, I.M.K., Faizal, K., Shukry, H.B. M., 2016. Rice yield estimation using below cloud remote sensing images acquired by unmanned airborne vehicle system. Int. J. Adv. Sci. Eng. Inf. Technol. 6 (4), 516–519.
Torres-Sanchez, J., Lopez-Granados, F., Pena, J.M., 2015. An automatic object-based method for optimal thresholding in UAV images: Application for vegetation detection in herbaceous crops. Comput. Electron. Agric. 114, 43–52.

Torres-Sánchez, J., Pe A, J.M., de Castro, A.I., López-Granados, F., 2014. Multi-temporal mapping of the vegetation fraction in early-season wheat fields using images from UAV. Comput. Electron. Agric. 103, 104–113.
Tucker, C.J., Holben, B.N., Elgin Jr., J.H., Mcmurtrey III, J.E., 1980. Relationship of spectral data to grain yield variation. Photogrammetric Eng. Remote Sens. 46, 657–666.
Verger, A., Vigneau, N., Chéron, C., Gilliot, J., Comar, A., Baret, F., 2014. Green area index from an unmanned aerial system over wheat and rapeseed crops. Remote Sens. Environ. 152, 654–664.
Wang, L., Tian, Y., Yao, X., Zhu, Y., Cao, W., 2014. Predicting grain yield and protein content in wheat by fusing multi-sensor and multi-temporal remote-sensing images. Field Crops Res. 164, 178–188.
Wang, Y.P., Chang, K.W., Chen, R.K., Jengchung, L., Yuan, S., 2010. Large-area rice yield forecasting using satellite imageries. Int. J. Appl. Earth Obs. Geoinf. 12 (1), 27–35.
Woebbecke, D.M., Meyer, G.E., Vonbargen, K., et al., 1995. Color indexes for weed identification under various soil, residue, and lighting conditions. Trans. ASAE 38 (1), 259–269.
Xue, L., Cao, W., Yang, L., 2007. Predicting grain yield and protein content in winter wheat at different N supply levels using canopy reflectance spectra. Pedosphere 17, 646–653.
Yang, C., Everitt, J.H., Bradford, J.M., 2006. Comparison of quickbird satellite imagery and airborne imagery for mapping grain sorghum yield patterns. Precision Agric. 7, 33–44.
Yang, C., Everitt, J.H., Bradford, J.M., 2009. Evaluating high resolution SPOT 5 satellite imagery to estimate crop yield. Precision Agric. 10, 292–303.
Zarco-Tejada, P.J., Gonzalez-Dugo, V., Berni, J.A.J., 2012. Fluorescence, temperature and narrow-band indices acquired from a UAV platform for water stress detection using a micro-hyperspectral imager and a thermal camera. Remote Sens. Environ. 117, 322–337.
Zarco-Tejada, P.J., Guillen-Climent, M.L., Hernandez-Clemente, R., Catalina, A., Gonzalez, M.R., Martin, P., 2013. Estimating leaf carotenoid content in vineyards using high resolution hyperspectral imagery acquired from an unmanned aerial vehicle (UAV). Agric. For. Meteorol. 171, 281–294.
Zhang, C., Kovacs, J.M., 2012. The application of small unmanned aerial systems for precision agriculture: a review. Precision Agric. 13, 693–712.
Zhao, D., Reddy, K.R., Kakani, V.G., Read, J.J., Koti, S., 2007. Canopy reflectance in cotton for growth assessment and lint yield prediction. Eur. J. Agron. 26, 335–344.
Xue, L., Cao, W., Luo, W., 2005. Rice yield forecasting model with canopy reflectance spectra. J. Remote Sens. 01, 100–105 (In Chinese).